
Neural Clustering Processes

Ari Pakman¹ Yueqi Wang^{1,2} Catalin Mitelut¹ JinHyung Lee¹ Liam Paninski¹

Abstract

Probabilistic clustering models (or equivalently, mixture models) are basic building blocks in countless statistical models and involve latent random variables over discrete spaces. For these models, posterior inference methods can be inaccurate and/or very slow. In this work we introduce deep network architectures trained with labeled samples from any generative model of clustered datasets. At test time, the networks generate approximate posterior samples of cluster labels for any new dataset of arbitrary size. We develop two complementary approaches to this task, requiring either $O(N)$ or $O(K)$ network forward passes per dataset, where N is the dataset size and K the number of clusters. Unlike previous approaches, our methods sample the labels of all the data points from a well-defined posterior, and can learn non-parametric Bayesian posteriors since they do not limit the number of mixture components. As a scientific application, we present a novel approach to neural spike sorting for high-density multielectrode arrays.

1. Introduction

Probabilistic clustering models (or equivalently, mixture models) are a staple of statistical modelling in which a discrete latent variable is introduced for each observation, indicating its mixture component identity. Popular inference methods in these models fall into two main classes. When exploring the full posterior is crucial (e.g. there is irreducible uncertainty about the latent structure or many separate local optima exist), the method of choice is Markov Chain Monte Carlo (MCMC) (Neal, 2000; Jain & Neal, 2004). This method is asymptotically accurate but time-consuming, with convergence that is difficult to assess. Models whose likelihood and prior are non-conjugate are par-

ticularly challenging, since in general in these cases the model parameters cannot be marginalized and must be kept as part of the state of the Markov chain. Alternatively, variational methods (Blei & Jordan, 2004; Kurihara et al., 2007; Hughes et al., 2015) are typically much faster but do not come with accuracy guarantees.

As a third alternative, in recent years there has been steady progress on amortized inference methods, and such is the spirit of this work. Concretely, we propose novel techniques to perform amortized approximate posterior inference over discrete latent variables in mixture models. We consider two possible product expansions of the mixture posteriors, and in each expansion we use neural networks to express conditional factors in terms of fixed-dimensional, distributed representations that respect the permutation symmetries imposed by the discrete variables. A major advantage of our approach, compared to previous approaches to amortized clustering, is its ability to handle an arbitrary number of clusters from a well defined posterior. This makes the methods a natural choice for nonparametric Bayesian models, such as Dirichlet process mixture models (DPMM), and their extensions. Moreover, the methods can be applied to both conjugate and non-conjugate models.

The term ‘amortization’ refers to the process of investing computational resources to train a model that is later used for very fast posterior inference (Gershman & Goodman, 2014). Concretely, in a model with observations x and latent variables z , the amortized approach learns a parametrized function $q_\theta(z|x)$ that approximates $p(z|x)$ for any x ; learning the parameters θ may be challenging, but once θ is in hand evaluating $q_\theta(z|x)$ for new data x is fast.

The amortized inference literature can be coarsely divided into two approaches. On one side, the variational autoencoder (VAE) approach (Kingma & Welling, 2013), with roots in the wake-sleep algorithm (Hinton et al., 1995), learns $q_\theta(z|x)$ along with the generative model $p_\phi(x|z)$. Here $p(z)$ is usually a known simple distribution.

Our work corresponds to the alternative case: a generative model $p(x, z)$ is postulated, and posterior inference is the main focus of the learning phase. Amortized methods in this case usually involve a degree of specialization to the particular generative model of interest. Examples include methods developed for Bayesian networks (Stuhmüller et al., 2013),

¹Columbia University ²Now at Google. Correspondence to: Ari Pakman <aripakman@gmail.com>.

sequential Monte Carlo (Paige & Wood, 2016), probabilistic programming (Ritchie et al., 2016; Le et al., 2016), neural decoding (Parthasarathy et al., 2017) and particle tracking (Sun & Paninski, 2018). Our work is specialized to the case where the latent variables are discrete and their range is not fixed beforehand.

After training a neural architecture using labeled samples from a particular generative model, we can obtain independent, parallelizable, approximate posterior samples of the discrete variables for any new set of observations of arbitrary size, with no need for expensive MCMC steps. These samples can be used (i) to approximate expectations, (ii) as high quality importance samples, or (iii) as independent Metropolis-Hastings proposals.

In Section 2 we introduce generative mixture models and present two distinct expansions of the posterior distribution. In Section 3 and Section 4 we present neural architectures to model the factors of each expansion, along with their objective functions. In Section 5 we present two simple examples to illustrate the methods. In Section 6 we review related works. In Section 7 we discuss quantitative evaluations of the new methods. We close in Section 8 with a neuroscientific application to spike sorting for high-density multielectrode probes. The Supplementary Material (SM) contains details on the architectures, the spike-sorting application, and an extension of these ideas to particle tracking.¹

2. Generative Mixture Models

We start by presenting mixture models from the perspective of probabilistic models for clustering (McLachlan & Basford, 1988). The latter introduce random variables c_i denoting the cluster number to which the data point x_i is assigned, and assume a generating process of the form

$$\begin{aligned} \alpha_1, \alpha_2 &\sim p(\alpha) \\ N &\sim p(N) \\ c_1 \dots c_N &\sim p(c_1, \dots, c_N | \alpha_1) \\ \mu_1 \dots \mu_K | c_{1:N} &\sim p(\mu_1, \dots, \mu_K | \alpha_2) \\ x_i &\sim p(x_i | \mu_{c_i}) \quad i = 1 \dots N. \end{aligned} \quad (1)$$

Here α_1, α_2 are hyperparameters. The number of clusters K is a random variable, indicating the number of distinct values among the sampled c_i 's, and μ_k denotes a parameter vector controlling the distribution of the k -th cluster (e.g., μ_k could include both the mean and covariance of a Gaussian mixture component). We assume that the priors $p(c_{1:N} | \alpha_1)$ and $p(\mu_{1:K} | \alpha_2)$ are exchangeable,

$$p(c_1, \dots, c_N | \alpha_1) = p(c_{\sigma_1}, \dots, c_{\sigma_N} | \alpha_1),$$

¹An early version appeared in (Pakman & Paninski, 2018; Wang et al., 2019). Similar methods were applied to amortized permutations in (Pakman et al., 2019).

where $\{\sigma_i\}$ is an arbitrary permutation of the indices, and similarly for $p(\mu_{1:K} | \alpha_2)$. Our interest in this work is in cases where K can take any value $K \leq N$, such as the Chinese Restaurant Process (CRP) or its Pitman-Yor generalization (see Rodriguez & Mueller (2013) for a review). Of course, our methods will also work for models with $K < B$ with fixed B , such as Mixtures of Finite Mixtures (Miller & Harrison, 2018).

Instead of representing configurations using N labels c_i , an alternative is obtained using K sets of *indices*:

$$\begin{aligned} \mathbf{s}_k &= (s_{k,1}, \dots, s_{k,N_k}) \quad k = 1 \dots K, \quad (2) \\ \text{where} \quad &\forall k, \forall i, c_{s_{k,i}} = k. \end{aligned}$$

For example, the labels $c_{1:6} = (1, 1, 2, 1, 2, 1)$ are equivalent to $\mathbf{s}_1 = (1, 2, 4, 6)$, $\mathbf{s}_2 = (3, 5)$. Note that cluster k has size N_k and $N = \sum_{k=1}^K N_k$. Given N data points $\mathbf{x} = \{x_i\}$, we would like to draw independent samples from the posterior $p(\mathbf{c} | \mathbf{x})$. For this, we consider expanding $p(\mathbf{c} | \mathbf{x})$ using either the labels representation,

$$p(c_{1:N} | \mathbf{x}) = p(c_1 | \mathbf{x}) p(c_2 | c_1, \mathbf{x}) \dots p(c_N | c_{1:N-1}, \mathbf{x}), \quad (3)$$

or the indices representation,

$$p(\mathbf{s}_{1:K} | \mathbf{x}) = p(\mathbf{s}_1 | \mathbf{x}) p(\mathbf{s}_2 | \mathbf{s}_1, \mathbf{x}) \dots p(\mathbf{s}_K | \mathbf{s}_{1:K-1}, \mathbf{x}). \quad (4)$$

Note that for a given cluster configuration, $p(c_{1:N} | \mathbf{x}) = p(\mathbf{s}_{1:K} | \mathbf{x})$. In the next two Sections, we present neural architectures to model the factors in each of these expansions.

3. Pointwise Sampling

We would like to model all the factors in (3) in a unified way, with a generic factor given by

$$p(c_n | c_{1:n-1}, \mathbf{x}) = \frac{p(c_1 \dots c_n, \mathbf{x})}{\sum_{c'_n=1}^{K+1} p(c_1 \dots c'_n, \mathbf{x})}. \quad (5)$$

Here we assumed that there are K unique values in $c_{1:n-1}$, and therefore c_n can take $K + 1$ values, corresponding to x_n joining any of the K existing clusters, or forming its own new cluster.

Since (5) is in general difficult to compute directly, we will approximate these terms with a neural network $q_\theta(c_n | c_{1:n-1}, \mathbf{x})$, that takes as inputs $(c_{1:n-1}, \mathbf{x})$, then extracts features and combines them nonlinearly to output a probability distribution on c_n . Critically, we will design the network to enforce the highly symmetric structure of (5).

To make this symmetric structure more transparent, let us consider the joint distribution of the assignments of the first n data points,

$$p(c_1, \dots, c_n, \mathbf{x}). \quad (6)$$

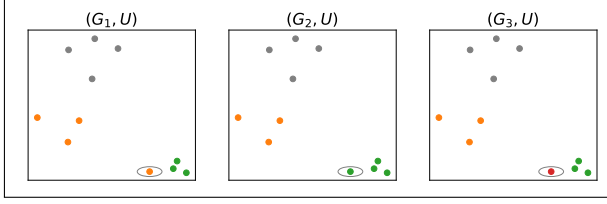


Figure 1. **Encoding cluster labels.** After assigning labels $c_{1:6}$ to $K = 2$ clusters, each of the three possible c_7 labels (for the circled point x_7) gives an encoding G_k for the set $x_{1:7}$. The vector U encodes the four gray unlabeled points (Best in color).

Note that under the model (1), this quantity depends on all the N elements of \mathbf{x} , not just on $x_{1:n}$. A neural representation of (6) should respect the permutation symmetries imposed on the x_i 's by the values of $c_{1:n}$. Therefore, our first task is to build permutation-invariant representations of the observations \mathbf{x} . The general problem of constructing such invariant encodings was discussed recently in (Zaheer et al., 2017); to adapt this approach to our context, we consider three distinct permutation symmetries:

- **Permutations within a cluster:** (6) is invariant under permutations of x_i 's in the same cluster. For each of the K clusters that have been sampled so far, we define the encoding

$$H_k = \sum_{i:c_i=k} h(x_i) \quad h: \mathbb{R}^{d_x} \rightarrow \mathbb{R}^{d_h} \quad (7)$$

which is clearly invariant under permutations of x_i 's in the same cluster. In general h is an encoding function we learn from data, unless $p(x|\mu)$ belongs to an exponential family and the prior $p(c_{1:N})$ is constant, as discussed in SM Section B.

- **Permutations between clusters:** (6) is invariant under permutations of the cluster labels. In terms of the within-cluster invariants H_k , this can be captured by

$$G = \sum_{k=1}^K g(H_k), \quad g: \mathbb{R}^{d_h} \rightarrow \mathbb{R}^{d_g}. \quad (8)$$

- **Permutations of the unassigned data points:** (6) is also invariant under permutations of the $N - n$ unassigned data points. This can be captured by

$$U = \sum_{i=n+1}^N u(x_i), \quad u: \mathbb{R}^{d_x} \rightarrow \mathbb{R}^{d_u}. \quad (9)$$

Note that G and U provide fixed-dimensional, symmetry-invariant representations of the assigned and non-assigned data points, respectively, for any values of N and K . Encodings of this form yield arbitrarily accurate approximations

of (partially) symmetric functions (Zaheer et al., 2017; Gui et al., 2019).

3.1. The Variable-input Softmax

After assigning values to $c_{1:n-1}$, each of the $K + 1$ possible values for c_n corresponds to $h(x_n)$ appearing in one particular H_k in (7), and yields a separate vector G_k in (8). See Figure 1 for an example. In terms of the G_k 's and U , we propose to model (5) as

$$q_\theta(c_n = k | c_{1:n-1}, \mathbf{x}) = \frac{e^{f(G_k, U)}}{\sum_{k'=1}^{K+1} e^{f(G_{k'}, U)}} \quad (10)$$

with $k = 1 \dots K + 1$, where we have introduced a new real-valued function f . In other words, each value of c_n corresponds to a different channel through which the encoding $h(x_n)$ flows to the logit value f . Note that $k = K + 1$ corresponds to c_n forming its own new cluster with $H_k = h(x_n)$.

Our softmax (10) differs from the usual form in, e.g., classification networks, where a fixed number of categories receive logit values f from the fixed-size final layer of a multi-layer perceptron (MLP). In our case, the discrete identity of each logit is determined by the neural path that the input $h(x_n)$ takes to G , thus allowing a flexible number of categories.

In eq. (10), θ denotes the parameters in the functions h, g, u and f , which we represent with neural networks. By storing and updating G and U for successive values of n , as shown in Algorithm 1, the computational cost of a full i.i.d. sample of $c_{1:N}$ is $O(NK)$, the same as a single Gibbs sweep; and by parallelizing steps 8-9 in Algorithm 1, the number of network forward passes becomes $O(N)$. We term this approach Neural Clustering Process (NCP). It is relatively easy to run hundreds of copies of Algorithm 1 in parallel on a GPU, with each copy yielding a different set of samples $c_{1:N}$.²

3.2. Objective Function

In order to train the neural networks, we use stochastic gradient descent to minimize the expected KL divergence,

$$\mathbb{E}_{p(N)p(\mathbf{x})} KL(p(c|\mathbf{x}) || q_\theta(c|\mathbf{x})) = \quad (11)$$

$$-\mathbb{E}_{p(N)p(c_{1:N}, \mathbf{x})} \left[\sum_{n=2}^N \log q_\theta(c_n | c_{1:n-1}, \mathbf{x}) \right] + \text{const.}$$

Samples from $p(c_{1:N}, \mathbf{x})$ are obtained from the generative model, irrespective of the model being conjugate. In cases with unlimited samples (such as the 2D Gaussian example in Section 5 and the spike-sorting application in Section 8), we can potentially train a neural network to approximate $p(c_n | c_{1:n-1}, \mathbf{x})$ arbitrarily accurately.

The objective function (11) can be seen as a form of Expectation Propagation (Minka, 2001), as opposed

²Implementation available at https://github.com/aripakman/neural_clustering_process

Algorithm 1 $O(NK)$ Neural Clustering Process

```

1:  $h_i \leftarrow h(x_i)$ ,  $u_i \leftarrow u(x_i)$     $i = 1 \dots N$  {Notation}
2:  $U \leftarrow \sum_{i=2}^N u_i$ ,  $K \leftarrow 1$    {Initialize unassigned set}
3:  $H_1 \leftarrow h_1$ ,  $G \leftarrow g(H_1)$ ,  $c_1 \leftarrow 1$    {First cluster}
4: for  $n \leftarrow 2 \dots N$  do
5:    $U \leftarrow U - u_n$    {Remove  $x_n$  from unassigned set}
6:    $H_{K+1} \leftarrow 0$    {We define  $g(0) = 0$ }
7:   for  $k \leftarrow 1 \dots K + 1$  do
8:      $G_k \leftarrow G + g(H_k + h_n) - g(H_k)$    {Add  $x_n$ }
9:      $q_k \leftarrow e^{f(G_k, U)}$ 
10:  end for
11:   $q_k \leftarrow q_k / \sum_{k'=1}^{K+1} q_{k'}$ ,  $c_n \sim q_k$    {Sample}
12:  if  $c_n = K + 1$  then
13:     $K \leftarrow K + 1$ 
14:  end if
15:   $G \leftarrow G - g(H_{c_n}) + g(H_{c_n} + h_n)$  {Add point  $x_n$ }
16:   $H_{c_n} \leftarrow H_{c_n} + h_n$ 
17: end for
18: Return  $c_1 \dots c_N$ 

```

to variational inference, which would minimize instead $KL(q_\theta(c|\mathbf{x})\|p(c|\mathbf{x}))$. Note that the gradient acts only on the variable-input softmax q_θ , not on $p(c, \mathbf{x})$, so there is no problem of backpropagating through discrete variables (Jang et al., 2016; Maddison et al., 2016).

4. Clusterwise Sampling

While the NCP algorithm is good enough for small datasets, $O(N)$ forward calls might be too many for large datasets. We consider now an $O(K)$ alternative, based on modeling the factors in the clusterwise expansion (4),

$$p(\mathbf{s}_{1:K}|\mathbf{x}) = p(\mathbf{s}_1|\mathbf{x})p(\mathbf{s}_2|\mathbf{s}_1, \mathbf{x}) \dots p(\mathbf{s}_K|\mathbf{s}_{1:K-1}, \mathbf{x}). \quad (12)$$

Sampling from $p(\mathbf{s}_k|\mathbf{s}_{1:k-1}, \mathbf{x})$ can be done in two steps:

1. Sample uniformly an index d_k from the set $I_k = \{1 \dots N\} \setminus \{\mathbf{s}_{1:k-1}\}$ of available indices (those not taken by $\mathbf{s}_{1:k-1}$). The point x_{d_k} becomes the first element of cluster k .
2. Denote by $\mathbf{a}_k = (a_1 \dots a_{m_k})$ the elements of the set of remaining indices $I_k \setminus \{d_k\}$, where $m_k = |I_k \setminus \{d_k\}|$. Conditioned on $(d_k, \mathbf{s}_{1:k-1}, \mathbf{x})$, sample a binary vector

$$\mathbf{b}_k = (b_1 \dots b_{m_k}) \in \{0, 1\}^{m_k}$$

with $b_i = 1$ if the point x_{a_i} joins cluster k .

These two steps (see Figure 2 for an example) are iterated until there are no available indices left, and have probability

$$p(d_k, \mathbf{b}_k|\mathbf{s}_{1:k-1}, \mathbf{x}) = p(d_k|\mathbf{s}_{1:k-1})p(\mathbf{b}_k|d_k, \mathbf{s}_{1:k-1}, \mathbf{x}) \quad (13)$$

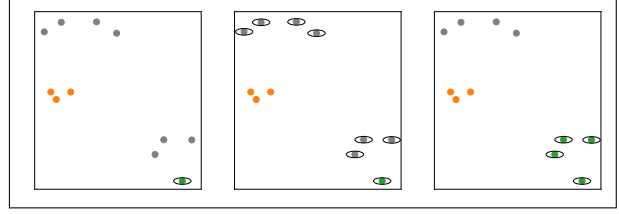


Figure 2. **Clusterwise sampling.** *Left:* After sampling cluster \mathbf{s}_1 (orange), the first element of \mathbf{s}_2 , d_2 , is sampled uniformly (green). *Middle:* All unassigned points \mathbf{a}_2 (grey) are candidates to join d_2 . *Right:* By sampling \mathbf{b}_2 , cluster \mathbf{s}_2 is completed. (Best in color).

where

$$p(d_k|\mathbf{s}_{1:k-1}) = \begin{cases} 1/|I_k| & \text{for } d_k \in I_k, \\ 0 & \text{for } d_k \notin I_k, \end{cases}$$

and $|I_k| = m_k + 1$. The event indicated by \mathbf{s}_k is the union of N_k disjoint events (d_k, \mathbf{b}_k) , and we have

$$p(\mathbf{s}_k|\mathbf{s}_{1:k-1}, \mathbf{x}) = \frac{1}{|I_k|} \sum_{d_k \in \mathbf{s}_k} p(\mathbf{b}_k|d_k, \mathbf{s}_{1:k-1}, \mathbf{x}) \quad (14)$$

where \mathbf{b}_k has a ‘1’ for each element in \mathbf{s}_k except d_k . Our major challenge is therefore to model the conditional $p(\mathbf{b}_k|d_k, \mathbf{s}_{1:k-1}, \mathbf{x})$, which we address next.

4.1. Factorized posterior

The information contained in $(d_k, \mathbf{s}_{1:k-1}, \mathbf{x})$, is better represented by splitting the dataset as $\mathbf{x}_k = (\mathbf{x}_a, x_{d_k}, \mathbf{x}_s)$, where

$$\begin{aligned} \mathbf{x}_a &= (x_{a_1} \dots x_{a_{m_k}}) && m_k \text{ available points for cluster } k \\ x_{d_k} &&& \text{First data point in cluster } k \\ \mathbf{x}_s &= (\mathbf{x}_{s_1} \dots \mathbf{x}_{s_{k-1}}) && \text{Points already assigned to clusters.} \end{aligned}$$

Thus $p(\mathbf{b}_k|\mathbf{x}_k) \equiv p(\mathbf{b}_k|d_k, \mathbf{s}_{1:k-1}, \mathbf{x})$. Note now that this factor has a form of conditional exchangeability

$$\begin{aligned} p(b_1 \dots b_{m_k} | x_{a_1}, \dots, x_{a_{m_k}}, x_{d_k}, \mathbf{x}_s) &= \\ p(b_{\sigma_1} \dots b_{\sigma_{m_k}} | x_{\sigma_{a_1}} \dots x_{\sigma_{a_{m_k}}}, x_{d_k}, \mathbf{x}_s), \end{aligned}$$

where σ is an arbitrary permutation of the elements of \mathbf{b}_k and \mathbf{x}_a . Based on this, we assume a conditional version of de Finetti’s theorem and propose³

$$p(\mathbf{b}_k|\mathbf{x}_k) \simeq \int d\mathbf{z}_k \prod_{i=1}^{m_k} p_i(b_i|\mathbf{z}_k, \mathbf{x}_k) p(\mathbf{z}_k|\mathbf{x}_k), \quad (15)$$

³More precisely, de Finetti’s theorem (de Finetti, 1931; Hewitt & Savage, 1955) holds for infinite sequences. For finite sequences, as in our case, the result has been shown to hold only approximately and for discrete variables, both in the unconditional (Diaconis, 1977; Diaconis & Freedman, 1980) and conditional cases (Christandl & Toner, 2009).

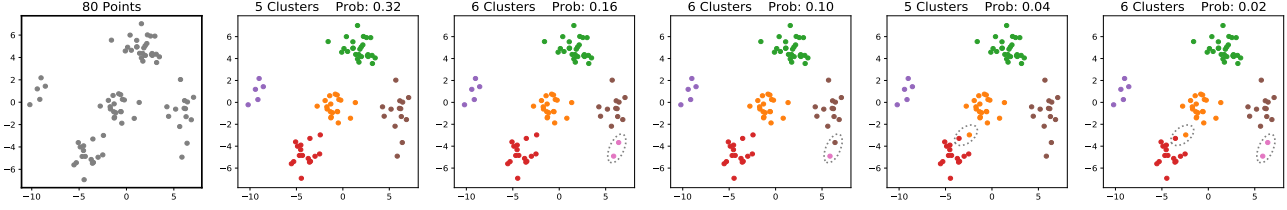


Figure 3. **Mixture of 2D Gaussians:** Given the observations in the first panel, we show samples from the NCP posterior. Note that less-reasonable samples are assigned lower probability by the NCP. The dotted ellipses indicate departures from the first, highest-probability sample. Our GPU implementation gives thousands of samples in less than a second. CCP results are similar. (Best in color.)

and approximate the integrands as

$$p_{\theta}(\mathbf{z}_k | \mathbf{x}_k) = \mathcal{N}(\mathbf{z}_k | \mathbf{x}_k) \quad (16)$$

$$p_{\theta,i}(b_i | \mathbf{z}_k, \mathbf{x}_k) = \text{sigmoid}[\rho_i(\mathbf{z}_k, \mathbf{x}_k)]. \quad (17)$$

Crucially, the posterior distributions of the b_i 's are conditionally independent. Therefore, after sampling $p(\mathbf{z}_k | \mathbf{x}_k)$, all the b_i 's can be sampled in parallel. Thus, while a full sample of (12) of course has cost $O(N)$, the heaviest computational burden, from network evaluations, scales as $O(K)$, since each factor in (12) needs $O(1)$ forward calls. As in NCP, we can get hundreds of full samples via GPU parallelization.

To summarize, the elements of \mathbf{s}_k are generated in a process with latent variables d_k, \mathbf{z}_k and joint distribution

$$p_{\theta}(\mathbf{s}_k, \mathbf{z}_k, d_k | \mathbf{s}_{1:k-1}, \mathbf{x}) = p_{\theta}(\mathbf{b}_k | \mathbf{z}_k, \mathbf{x}_k) p_{\theta}(\mathbf{z}_k | \mathbf{x}_k) p(d_k | \mathbf{s}_{1:k-1})$$

where

$$p_{\theta}(\mathbf{b}_k | \mathbf{z}_k, \mathbf{x}_k) = \prod_{i=1}^{m_k} p_{\theta,i}(b_i | \mathbf{z}_k, \mathbf{x}_k). \quad (18)$$

In order to learn these functions, we introduce an encoder $q_{\phi}(\mathbf{z}_k, d_k | \mathbf{s}_{1:k}, \mathbf{x})$ to approximate the intractable posterior, and train the functions as a conditional variational autoencoder (VAE) (Sohn et al., 2015) (as we condition everything on \mathbf{x}). The dependence of all the functions on the components of \mathbf{x} should respect the symmetries imposed by the conditioning clusters $\mathbf{s}_{1:k-1}$ (or $\mathbf{s}_{1:k}$ for q_{ϕ}). This can be achieved using encodings similar to those we used above in Section 3; see SM Section A for details.

Let us stress the double role of $p_{\theta}(\mathbf{z}_k | \mathbf{x}_k) p(d_k | \mathbf{s}_{1:k-1})$ and $p_{\theta}(\mathbf{b}_k | \mathbf{z}_k, \mathbf{x}_k)$. In the VAE framework, they are the priors and likelihood of a generative model for \mathbf{s}_k . On the other hand they represent, after d_k, \mathbf{z}_k marginalization (14)-(15), a factor of the posterior expansion (12). We call this approach Clusterwise Clustering Process (CCP).

4.2. Objective Function

Similar to the NCP case in (11), we want an approximation $p_{\theta}(\mathbf{s}_{1:K} | \mathbf{x})$ to $p(\mathbf{s}_{1:K} | \mathbf{x})$ that maximizes

$$-\mathbb{E}_{p(\mathbf{x})} KL[p(\mathbf{s}_{1:K} | \mathbf{x}) || p_{\theta}(\mathbf{s}_{1:K} | \mathbf{x})] \quad (19)$$

$$= \mathbb{E}_{p(\mathbf{x}, \mathbf{s}_{1:K})} \sum_{k=1}^K \log p_{\theta}(\mathbf{s}_k | \mathbf{s}_{1:k-1}, \mathbf{x}) + \text{const.}$$

where we expanded $p_{\theta}(\mathbf{s}_{1:K} | \mathbf{x})$ as in (12). Using now the variational posterior q_{ϕ} , we can bound (19) from below, which leads us to maximize the ELBO

$$\mathbb{E}_{p(\mathbf{x}, \mathbf{s}_{1:K})} \sum_{k=1}^K \mathbb{E}_{q_{\phi}(\mathbf{z}_k, d_k | \mathbf{s}_{1:k}, \mathbf{x})} \log \left[\frac{p_{\theta}(\mathbf{s}_k, \mathbf{z}_k, d_k | \mathbf{s}_{1:k-1}, \mathbf{x})}{q_{\phi}(\mathbf{z}_k, d_k | \mathbf{s}_{1:k}, \mathbf{x})} \right]$$

To use the reparametrization trick (Kingma & Welling, 2013), we use a Gumbel-Softmax relaxation for d_k (Jang et al., 2016; Maddison et al., 2016). See SM Section A.

4.3. Estimating sample probabilities

Unlike NCP, CCP samples do not come with a probability estimate. The latter can be estimated using (12) and

$$p(\mathbf{b}_k | \mathbf{x}_k) \simeq \frac{1}{M} \sum_{j=1}^M p_{\theta}(\mathbf{b}_k | \mathbf{z}_{k,j}, \mathbf{x}_k) \quad (20)$$

where $\mathbf{z}_{k,j} \sim p_{\theta}(\mathbf{z}_k | \mathbf{x}_k)$.

5. Examples

2D Gaussian models: The generative model is

$$\alpha \sim \text{Exp}(1) \quad c_{1:N} \sim \text{CRP}(\alpha) \quad \mu_k \sim N(0, \sigma_{\mu}^2 \mathbf{1}_2)$$

$$N \sim \text{Uniform}[5, 100] \quad x_i \sim N(\mu_{c_i}, \sigma^2 \mathbf{1}_2)$$

where CRP stands for the Chinese Restaurant Process, with concentration parameter α , $\sigma_{\mu} = 10$, and $\sigma = 1$. Figure 3 shows that the NCP captures the posterior uncertainty inherent in clustering this data. Since we have unlimited samples, there is no distinction here between training and test sets.

MNIST digits: We consider next a DPMM over MNIST digits, with generative model

$$\alpha \sim \text{Exp}(1) \quad c_{1:N} \sim \text{CRP}_{10}(\alpha)$$

$$N \sim \text{Uniform}[5, 100]$$

$$l_k \sim \text{Unif}[0, 9] - \text{without replacement.} \quad k = 1 \dots K$$

$$x_i \sim \text{Unif}[\text{MNIST digits with label } l_{c_i}] \quad i = 1 \dots N$$

where CRP_{10} is a Chinese Restaurant Process truncated to up to 10 clusters, and $d_x = 28 \times 28$. Training was

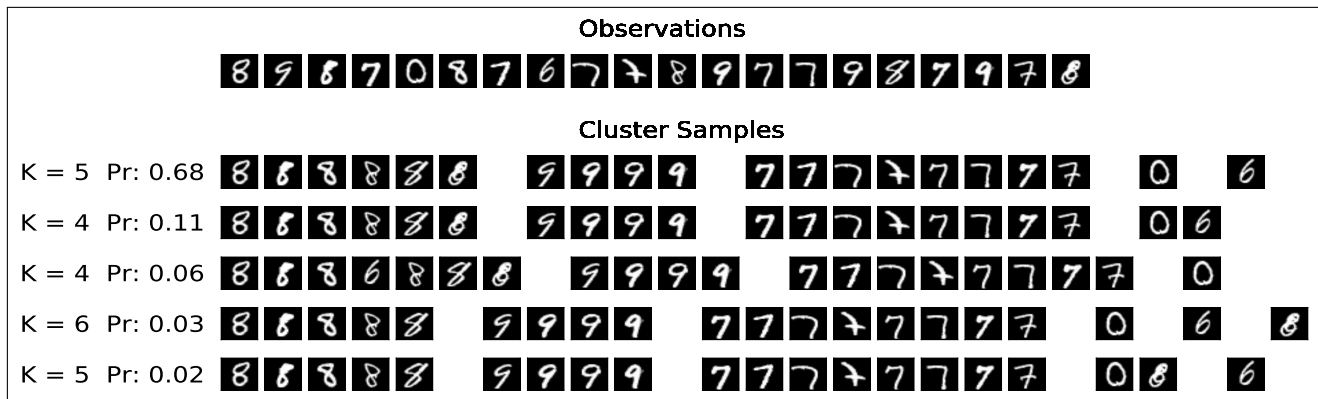


Figure 4. **NCP trained on MNIST clusters.** Top row: 20 images from the MNIST test set. Below: five samples of $c_{1:20}$ from the NCP posterior. Note that each sample captures some ambiguity suggested by the form of particular digits. CCP results are similar.

performed by sampling x_i from the MNIST training set. Figure 4 shows posterior samples for a set of digits from the MNIST test set, illustrating how the estimated model correctly captures the shape ambiguity of some of the digits. Note that in this case the generative model has no analytical expression, but this presents no problem; a set of labelled samples is all we need for training. See SM Section G for details of the network architectures used.

6. Related works

Most works on neural network-based clustering focus on learning features as inputs to traditional clustering algorithms, as reviewed in (Du, 2010; Aljalbout et al., 2018; Min et al., 2018). Our approach differs from these works because it leverages deep learning to improve *algorithmic* aspects of clustering, via amortization.

Permutation-invariant neural architectures have been explored recently in (Ravanbakhsh et al., 2017; Korshunova et al., 2018; Lee et al., 2018; Bloem-Reddy & Teh, 2019; Wagstaff et al., 2019). The representation of a set via a sum (or mean) of encoding vectors was also used in (Guttenberg et al., 2016; Ravanbakhsh et al., 2016; Edwards & Storkey, 2017; Zaheer et al., 2017; Garnelo et al., 2018a; Kim et al., 2019).

A conditional form of de Finetti’s theorem was also assumed for Neural Processes (NP) (Garnelo et al., 2018b), but differs from our assumed form in (15) in that our prior $p_\theta(\mathbf{z}_k | \mathbf{x}_k)$ depends symmetrically on the available points \mathbf{x}_a , in order to keep the correct dependency of the marginal $p(\mathbf{c}_{1:n}, \mathbf{x})$ on all the N components of \mathbf{x} , while for NPs the prior is independent of the available data points.

Amortized inference of Gaussian mixtures has been studied recently in (Le et al., 2016; Lee et al., 2018; Kalra et al., 2019). In these works the output of the network are the

mixture parameters instead of sampled discrete labels, and the number of components is either bounded (Le et al., 2016) or fixed (Lee et al., 2018; Kalra et al., 2019). Closer to our CCP is the DAC approach (Lee et al., 2019), that uses the set attention mechanism of (Lee et al., 2018) in the encoder to iteratively isolate and eliminate one cluster per iteration, in $O(K)$ network evaluations. But the clusters have no clear interpretation in terms of the generative model, as they come from hard thresholding of sigmoids and the eliminated clusters do not appear as a conditioning context to find new clusters. We summarize these comparisons in Table 1.

Property	CCP	NCP	DAC	MoG
Unlimited components	✓	✓	✓	✗
Amortized labels	✓	✓	✓	✗
Any generative model	✓	✓	✓	✗
Well defined posterior	✓	✓	✗	-
Forward passes	$O(K)$	$O(N)$	$O(K)$	$O(1)$

Table 1. **Comparing amortized clustering approaches.** We compare NCP/CCP (our methods) with DAC (Lee et al., 2019) and amortization for mixtures of Gaussians (MoG) (Le et al., 2016; Lee et al., 2018; Kalra et al., 2019).

7. Evaluations and diagnostics

The examples in Section 5 provide strong qualitative evidence that our approximations to the true posteriors in these models capture the uncertainty inherent in the observed data. But we would like to go further and ask quantitatively how well our approximations match the exact posterior. Unfortunately, for sample sizes much larger than $N = O(10)$ it is impossible to compute the exact posterior in these models. Nonetheless, there are several quantitative metrics we can examine to check the accuracy of the model output. Note that the diagnostics below that rely on the probabilistic nature of the inferred clusters are not applicable to the other

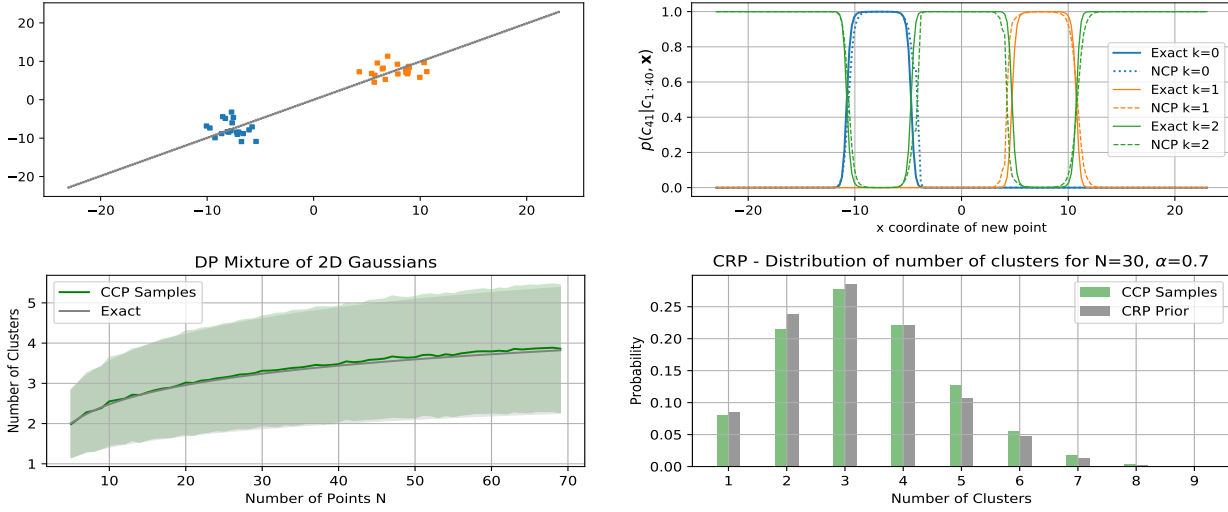


Figure 5. **Quantitative Evaluations.** *Upper left:* Two clusters of 20 points each and a line over possible locations of a 41st last point. *Upper right:* Assuming the 2D model from (21), the posterior $p(c_{41}|c_{1:40}, \mathbf{x})$ can be computed exactly, and we compare it to the NCP estimate as a function of the horizontal coordinate of x_{41} , as this point moves over the gray line on the upper left panel. *Geweke’s Tests.* *Lower left:* The curves compare the exact mean (\pm std.) of the number of clusters K for different N ’s from the CRP prior ($\alpha = 0.7$), with CCP sampled estimates using eq. (21). *Lower right:* Similar comparison for the histogram of K for $N = 30$ points.

methods compared in Table 1.

NCP vs. CCP: The results from the two approaches were similar in all the examples we considered, such as those in Section 5. Training CPP, however, presents the usual challenges of VAEs. We found it useful to use multiple sample objectives (Burda et al., 2015) and estimate the gradient using double-reparametrization (Tucker et al., 2019).

Global symmetry from exchangeability: From the exchangeability of $p(c_{1:N}|\alpha_1)$, the expansion (3) should not depend on the order of the data points, but this symmetry is not enforced explicitly. If our model learns the conditional probabilities correctly, this symmetry should be (approximately) satisfied, as we show in SM Section C.

Estimated vs. Analytical Probabilities: Some conditional probabilities can be computed analytically and compared with the estimates output by the network; in the example shown in Figure 5, upper-right, the estimated probabilities are in close agreement with their exact values.

Geweke’s Tests: A popular family of tests that check the correctness of MCMC implementations (Geweke, 2004) can also be applied in our case: verify the (approximate) identity between the prior $p(c_{1:N})$ and

$$q_{\theta}(c_{1:N}) \equiv \int d\mathbf{x} q_{\theta}(c_{1:N}|\mathbf{x}) p(\mathbf{x}), \quad (21)$$

where $p(\mathbf{x})$ is the marginal from the generative model. Figure 5 shows such a comparison for the 2D Gaussian DPMM from Section 5, showing excellent agreement.

Comparison with MCMC: NCP/CCP have some advantages over MCMC approaches. First, unlike MCMC, we get a probability estimate for each sample, either directly (NCP) or with minimal computation (CCP). Secondly, NCP/CCP enjoy higher efficiency, due to parallelization of iid samples. For example, in the Gaussian 2D example in eq.(21), in the time a collapsed Gibbs sampler produces one (correlated) sample, our GPU-based NCP implementation produces more than 100 iid approximate samples. Finally, NCP/CCP do not need a burn-in period.

Comparison with Variational Inference: Below we compare NCP with a variational approach on spike sorting. For 2000 spikes, the latter returned one clustering estimate in 0.76 secs., but does not properly handle the uncertainty about the number of clusters. NCP produced 150 clustering configurations in 10 secs., efficiently capturing clustering uncertainty. In addition, the variational approach requires a preprocessing step that projects the samples to lower dimensions, whereas NCP directly consumes the high-dimensional data by learning an encoder function h .

8. Application: spike sorting with NCP

Large-scale neural population recordings using multi-electrode arrays (MEA) are crucial for understanding neural circuit dynamics. Each MEA electrode reads the signals from many neurons, and each neuron is recorded by multiple nearby electrodes. As a key analysis step, spike sorting converts the raw signal into a set of spike trains belonging to individual neurons (Pachitariu et al., 2016; Chung et al.,

2017; Jun et al., 2017; Lee et al., 2017; Chaure et al., 2018; Carlson & Carin, 2019). At the core of many spike sorting pipelines is a clustering algorithm that groups the detected spikes into clusters, each representing a putative neuron (Figure 6). However, clustering spikes can be challenging: (1) Spike waveforms form highly non-Gaussian clusters in spatial and temporal dimensions, and it is unclear what are the optimal features for clustering. (2) It is unknown *a priori* how many clusters there are. (3) Existing methods do not perform well on spikes with low signal-to-noise ratios (SNR) due to increased clustering uncertainty, and fully-Bayesian approaches proposed to handle this uncertainty (Wood & Black, 2008; Carlson et al., 2013) do not scale to large datasets.

To address these challenges, we propose a novel approach to spike clustering using NCP. We consider the spike waveforms as generated from a Mixture of Finite Mixtures (MFM) distribution (Miller & Harrison, 2018), which can be effectively modeled by NCP. (1) Rather than selecting arbitrary features for clustering, the spike waveforms are encoded with a convolutional neural network (ConvNet), which is learned end-to-end jointly with the NCP network to ensure optimal feature encoding. (2) Using a variable-input softmax function, NCP is able to perform inference on cluster labels without assuming a fixed or maximum number of clusters. (3) NCP allows for efficient probabilistic clustering by GPU-parallelized posterior sampling, which is particularly useful for handling the clustering uncertainty of ambiguous small spikes. (4) The computational cost of NCP training can be highly amortized, since neuroscientists often sort spikes from many statistically similar datasets.

We trained NCP for spike clustering using synthetic spikes from a simple yet effective generative model that mimics the distribution of real spikes, and evaluated the spike sorting performance on labeled synthetic data, unlabeled real data and hybrid test data by comparing NCP against two other methods: (1) **vGMFM**, variational inference on Gaussian MFM (Hughes & Sudderth, 2013). (2) **Kilosort**, a state-of-the-art spike sorting pipeline described in (Pachitariu et al., 2016). In the Supplementary Material (SM) Section D, we describe the dataset, neural architecture, and the training/inference pipeline of NCP spike sorting. In SM Section E, we show that NCP spike sorting achieves high clustering quality, and matches or outperforms a state-of-the-art method on synthetic, real and hybrid data.

Probabilistic clustering of ambiguous small spikes. Sorting small spikes has been challenging due to the low SNR and increased uncertainty of cluster assignment. By efficient GPU-parallelized posterior sampling of cluster labels, NCP is able to handle the clustering uncertainty by producing multiple plausible clustering configurations. Figure 7 shows examples where NCP separates spike clusters with ampli-

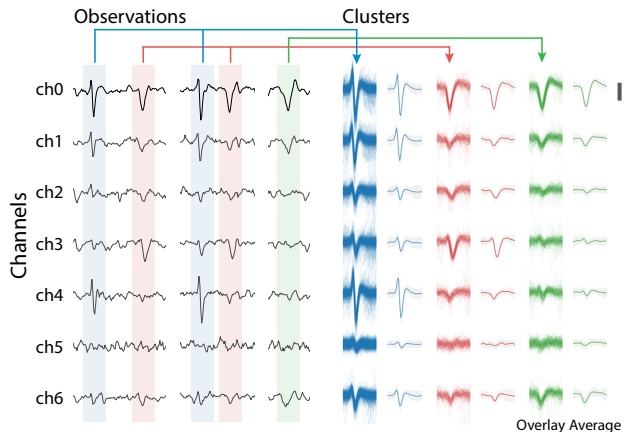


Figure 6. **Clustering multi-channel spike waveforms using NCP.** Each row is an electrode channel. Spikes of the same color belong to the same cluster. (Scale bar: $5 \times$ noise s.d.).

tude as low as $3-4 \times$ the standard deviation of the noise into plausible units that are not mere scaled version of each other but have distinct shapes on different channels. f

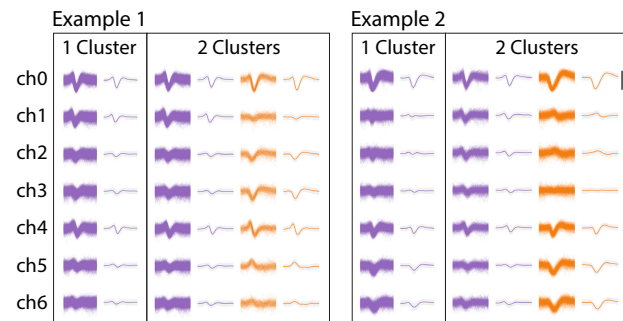


Figure 7. **Clustering ambiguous small spikes.** In both examples, multiple plausible clustering results of small spikes were produced by sampling from the NCP posterior (scale bar = $5 \times$ noise s.d.).

9. Conclusion

We introduced neural architectures to amortize posterior sampling of generative clustering models in $O(N)$ and $O(K)$ forward passes. The performance is excellent in simple examples. In a realistic spike-sorting application, our results show that NCP spike sorting provides high clustering quality, matches or outperforms a state-of-the-art method, and handles clustering uncertainty by efficient posterior sampling (a task that is not solved by currently available methods), demonstrating substantial promise for incorporating these methods into production-scale pipelines.

Acknowledgements

We thank Sean Bittner, Alessandro Ingrassio, Scott Linderman, Aaron Schein and Ruoxi Sun for helpful conversations. This work was supported by the Simons Foundation, the DARPA NESD program, ONR N00014-17-1-2843, NIH/NIBIB R01 EB22913, NSF NeuroNex Award DBI-1707398 and The Gatsby Charitable Foundation.

References

- Aljalbout, E., Golkov, V., Siddiqui, Y., and Cremers, D. Clustering with Deep Learning: Taxonomy and New Methods. *arXiv preprint arXiv:1801.07648*, 2018.
- Blei, D. M. and Jordan, M. I. Variational Methods for the Dirichlet Process. In *Proceedings of the Twenty-first International Conference on Machine Learning, ICML, 2004*.
- Bloem-Reddy, B. and Teh, Y. W. Probabilistic symmetry and invariant neural networks. *arXiv preprint arXiv:1901.06082*, 2019.
- Burda, Y., Grosse, R., and Salakhutdinov, R. Importance weighted autoencoders. *arXiv preprint arXiv:1509.00519*, 2015.
- Calabrese, A. and Paninski, L. Kalman filter mixture model for spike sorting of non-stationary data. *Journal of neuroscience methods*, 196(1):159–169, 2011.
- Carlson, D. and Carin, L. Continuing progress of spike sorting in the era of big data. *Current opinion in neurobiology*, 55:90–96, 2019.
- Carlson, D. E., Vogelstein, J. T., Wu, Q., Lian, W., Zhou, M., Stoetzner, C. R., Kipke, D., Weber, D., Dunson, D. B., and Carin, L. Multichannel electrophysiological spike sorting via joint dictionary learning and mixture modeling. *IEEE Transactions on Biomedical Engineering*, 61(1):41–54, 2013.
- Chahre, F. J., Rey, H. G., and Quian Quiroga, R. A novel and fully automatic spike-sorting implementation with variable number of features. *Journal of neurophysiology*, 120(4):1859–1871, 2018. doi: 10.1152/jn.00339.2018.
- Chichilnisky, E. J. and Kalmar, R. S. Functional asymmetries in on and off ganglion cells of primate retina. *Journal of Neuroscience*, 22(7):2737–2747, 2002. ISSN 0270-6474. doi: 10.1523/JNEUROSCI.22-07-02737.2002. URL <http://www.jneurosci.org/content/22/7/2737>.
- Christandl, M. and Toner, B. Finite de Finetti theorem for conditional probability distributions describing physical theories. *Journal of Mathematical Physics*, 50(4):042104, 2009.
- Chung, J. E., Magland, J. F., Barnett, A. H., Tolosa, V. M., Tooker, A. C., Lee, K. Y., Shah, K. G., Felix, S. H., Frank, L. M., and Greengard, L. F. A fully automated approach to spike sorting. *Neuron*, 95(6):1381–1394, 2017.
- de Finetti, B. Funzione caratteristica di un fenomeno aleatorio. *Atti della R. Accademia Nazionale dei Lincei, Serie 6. Memorie, Classe di Scienze Fisiche, Matematiche e Naturale*, 4, pp. 251–299, 1931.
- Diaconis, P. Finite forms of de Finetti’s theorem on exchangeability. *Synthese*, 36(2):271–281, 1977.
- Diaconis, P. and Freedman, D. Finite exchangeable sequences. *The Annals of Probability*, pp. 745–764, 1980.
- Du, K.-L. Clustering: A neural network approach. *Neural networks*, 23(1):89–107, 2010.
- Edwards, H. and Storkey, A. Towards a neural statistician. *ICLR*, 2017.
- Garnelo, M., Rosenbaum, D., Maddison, C. J., Ramalho, T., Saxton, D., Shanahan, M., Teh, Y. W., Rezende, D. J., and Eslami, S. Conditional neural processes. In *International Conference on Machine Learning*, 2018a.
- Garnelo, M., Schwarz, J., Rosenbaum, D., Viola, F., Rezende, D. J., Eslami, S., and Teh, Y. W. Neural processes. In *ICML 2018 workshop on Theoretical Foundations and Applications of Deep Generative Models*, 2018b.
- Gershman, S. and Goodman, N. Amortized inference in probabilistic reasoning. In *Proceedings of the annual meeting of the cognitive science society*, volume 36, 2014.
- Geweke, J. Getting it right: Joint distribution tests of posterior simulators. *Journal of the American Statistical Association*, 99(467):799–804, 2004.
- Graves, A. Sequence transduction with recurrent neural networks. *CoRR*, abs/1211.3711, 2012.
- Gui, S., Zhang, X., Zhong, P., Qiu, S., Wu, M., Ye, J., Wang, Z., and Liu, J. Pine: Universal deep embedding for graph nodes via partial permutation invariant set functions. *arXiv preprint arXiv:1909.12903*, 2019.
- Guttenberg, N., Virgo, N., Witkowski, O., Aoki, H., and Kanai, R. Permutation-equivariant neural networks applied to dynamics prediction. *arXiv preprint arXiv:1612.04530*, 2016.
- He, K., Zhang, X., Ren, S., and Sun, J. Deep residual learning for image recognition. In *The IEEE Conference on Computer Vision and Pattern Recognition (CVPR)*, June 2016.

- Hewitt, E. and Savage, L. J. Symmetric measures on cartesian products. *Transactions of the American Mathematical Society*, 80(2):470–501, 1955.
- Hinton, G. E., Dayan, P., Frey, B. J., and Neal, R. M. The “wake-sleep” algorithm for unsupervised neural networks. *Science*, 268(5214):1158–1161, 1995.
- Hughes, M., Kim, D. I., and Sudderth, E. Reliable and scalable variational inference for the hierarchical Dirichlet process. In *Artificial Intelligence and Statistics*, pp. 370–378, 2015.
- Hughes, M. C. and Sudderth, E. Memoized online variational inference for dirichlet process mixture models. In *Advances in Neural Information Processing Systems 26*, pp. 1133–1141. 2013.
- Jain, S. and Neal, R. M. A split-merge Markov chain Monte Carlo procedure for the Dirichlet process mixture model. *Journal of computational and Graphical Statistics*, 13(1): 158–182, 2004.
- Jang, E., Gu, S., and Poole, B. Categorical reparameterization with Gumbel-softmax. *arXiv preprint arXiv:1611.01144*, 2016.
- Jun, J. J., Mitelut, C., Lai, C., Gratiy, S. L., Anastassiou, C. A., and Harris, T. D. Real-time spike sorting platform for high-density extracellular probes with ground-truth validation and drift correction. *bioRxiv*, 2017.
- Kalra, S., Adnan, M., Taylor, G., and Tizhoosh, H. Learning permutation invariant representations using memory networks. *arXiv preprint arXiv:1911.07984*, 2019.
- Kim, H., Mnih, A., Schwarz, J., Garnelo, M., Eslami, A., Rosenbaum, D., Vinyals, O., and Teh, Y. W. Attentive neural processes. *ICLR*, 2019.
- Kingma, D. P. and Ba, J. Adam: A method for stochastic optimization. *ICLR*, 2015.
- Kingma, D. P. and Welling, M. Auto-encoding variational bayes. *arXiv preprint arXiv:1312.6114*, 2013.
- Korshunova, I., Degraeve, J., Huszar, F., Gal, Y., Gretton, A., and Dambre, J. Bruno: A deep recurrent model for exchangeable data. In *Advances in Neural Information Processing Systems 31*, 2018.
- Kurihara, K., Welling, M., and Teh, Y. W. Collapsed Variational Dirichlet Process Mixture Models. In *IJCAI*, volume 7, pp. 2796–2801, 2007.
- Le, T. A., Baydin, A. G., and Wood, F. Inference compilation and universal probabilistic programming. *arXiv preprint arXiv:1610.09900*, 2016.
- Lee, J., Lee, Y., Kim, J., Kosiorek, A. R., Choi, S., and Teh, Y. W. Set transformer. *arXiv preprint arXiv:1810.00825*, 2018.
- Lee, J., Lee, Y., and Teh, Y. W. Deep Amortized Clustering. *arXiv:1909.13433*, 2019.
- Lee, J. H., Carlson, D. E., Razaghi, H. S., Yao, W., Goetz, G. A., Hagen, E., Batty, E., Chichilnisky, E., Einevoll, G. T., and Paninski, L. Yass: Yet another spike sorter. In *Advances in Neural Information Processing Systems*, pp. 4002–4012, 2017.
- Maddison, C. J., Mnih, A., and Teh, Y. W. The concrete distribution: A continuous relaxation of discrete random variables. *arXiv preprint arXiv:1611.00712*, 2016.
- McLachlan, G. J. and Basford, K. E. *Mixture models: Inference and applications to clustering*, volume 84. Marcel Dekker, 1988.
- Miller, J. W. and Harrison, M. T. Mixture models with a prior on the number of components. *Journal of the American Statistical Association*, 113(521):340–356, 2018.
- Min, E., Guo, X., Liu, Q., Zhang, G., Cui, J., and Long, J. A survey of clustering with deep learning: From the perspective of network architecture. *IEEE Access*, 6: 39501–39514, 2018.
- Minka, T. P. Expectation propagation for approximate Bayesian inference. In *Proceedings of the Seventeenth conference on Uncertainty in artificial intelligence*, pp. 362–369. Morgan Kaufmann Publishers Inc., 2001.
- Neal, R. M. Markov chain sampling methods for Dirichlet process mixture models. *Journal of computational and graphical statistics*, 9(2):249–265, 2000.
- Pachitariu, M. Kilosort2. <https://github.com/MouseLand/Kilosort2>, 2019.
- Pachitariu, M., Steinmetz, N., Kadir, S., Carandini, M., and Harris, K. D. Kilosort: realtime spike-sorting for extracellular electrophysiology with hundreds of channels. *BioRxiv*, pp. 061481, 2016.
- Paige, B. and Wood, F. Inference networks for sequential Monte Carlo in graphical models. In *International Conference on Machine Learning*, pp. 3040–3049, 2016.
- Pakman, A. and Paninski, L. Amortized Bayesian inference for clustering models. *BNP@NeurIPS 2018 Workshop All of Bayesian Nonparametric*, 2018.
- Pakman, A., Wang, Y., and Paninski, L. Neural Permutation Processes. In *Symposium on Advances in Approximate Bayesian Inference*, pp. 1–7, 2019.

- Parthasarathy, N., Batty, E., Falcon, W., Rutten, T., Rajpal, M., Chichilnisky, E., and Paninski, L. Neural Networks for Efficient Bayesian Decoding of Natural Images from Retinal Neurons. In *Advances in Neural Information Processing Systems 30*, pp. 6434–6445, 2017.
- Ravanbakhsh, S., Schneider, J., and Poczos, B. Deep learning with sets and point clouds. *arXiv preprint arXiv:1611.04500*, 2016.
- Ravanbakhsh, S., Schneider, J., and Póczos, B. Equivariance through parameter-sharing. In *Proceedings of the 34th International Conference on Machine Learning*, 2017.
- Ritchie, D., Horsfall, P., and Goodman, N. D. Deep amortized inference for probabilistic programs. *arXiv preprint arXiv:1610.05735*, 2016.
- Rodriguez, A. and Mueller, P. NONPARAMETRIC BAYESIAN INFERENCE. *NSF-CBMS Regional Conference Series in Probability and Statistics*, 9:i–110, 2013.
- Shan, K. Q., Lubenov, E. V., and Siapas, A. G. Model-based spike sorting with a mixture of drifting t-distributions. *Journal of neuroscience methods*, 288:82–98, 2017.
- Sohn, K., Lee, H., and Yan, X. Learning structured output representation using deep conditional generative models. In *Advances in neural information processing systems*, pp. 3483–3491, 2015.
- Stuhlmüller, A., Taylor, J., and Goodman, N. Learning stochastic inverses. In *Advances in neural information processing systems*, pp. 3048–3056, 2013.
- Sun, R. and Paninski, L. Scalable approximate Bayesian inference for particle tracking data. In *Proceedings of the 35th International Conference on Machine Learning*, 2018.
- Sutskever, I., Vinyals, O., and Le, Q. V. Sequence to sequence learning with neural networks. In *NIPS*, 2014.
- Tucker, G., Lawson, D., Gu, S., and Maddison, C. J. Doubly reparameterized gradient estimators for monte carlo objectives. In *International Conference on Learning Representations*, 2019. URL <https://openreview.net/forum?id=HkG3e205K7>.
- Vinh, N. X., Epps, J., and Bailey, J. Information theoretic measures for clusterings comparison: Variants, properties, normalization and correction for chance. *Journal of Machine Learning Research*, 11(Oct):2837–2854, 2010.
- Wagstaff, E., Fuchs, F. B., Engelcke, M., Posner, I., and Osborne, M. On the limitations of representing functions on sets. *arXiv preprint arXiv:1901.09006*, 2019.
- Wang, Y., Pakman, A., Mitelut, C., Lee, J., and Paninski, L. Spike sorting using the neural clustering process. *Real Neurons & Hidden Units Workshop @ NeurIPS 2019*, 2019.
- Wood, F. and Black, M. J. A nonparametric bayesian alternative to spike sorting. *Journal of neuroscience methods*, 173(1):1–12, 2008.
- Zaheer, M., Kottur, S., Ravanbakhsh, S., Póczos, B., Salakhutdinov, R., and Smola, A. J. Deep sets. In *Advances in neural information processing systems*, 2017.

A. Details of the CCP Model

A.1. Encodings

In order to parametrize the prior, likelihood and posterior of the CCP model, it is convenient to define first some symmetric encodings for different subsets of the data set \mathbf{x} at iteration k . Remember that the notation \mathbf{x}_k indicates that the dataset is split into three groups, $\mathbf{x}_k = (\mathbf{x}_a, x_{d_k}, \mathbf{x}_s)$, where

$$\begin{aligned} \mathbf{x}_a &= (x_{a_1} \dots x_{a_{m_k}}) && m_k \text{ available points for cluster } k \\ x_{d_k} &&& \text{First data point in cluster } k \\ \mathbf{x}_s &= (\mathbf{x}_{s_1} \dots \mathbf{x}_{s_{k-1}}) && \text{Points already assigned to clusters.} \end{aligned}$$

The symmetric encodings we need are:

Definition	Encoded Points
$D_k = \sum_{i=1}^{N_k} \delta_{s_k, i, d_k} u(x_{s_k, i})$	x_{d_k} , the first point in cluster k
$A_k^{in} = \sum_{i=1}^{N_k} (1 - \delta_{s_k, i, d_k}) u(x_{s_k, i})$	Points from \mathbf{x}_a that join cluster k .
$A_k^{out} = \sum_{i=1, b_i=0}^{m_k} u(x_{a_i})$	Points from \mathbf{x}_a that do not join cluster k
$A_k = A_k^{in} + A_k^{out}$	\mathbf{x}_a , all the m_k points available to join x_{d_k}
$S_k = D_k + A_k^{in}$	All points s_k in cluster k
$H_j = \sum_{x: x \in s_j} h(x) \quad j = 1 \dots k-1$	All points in cluster $j < k$
$G_k = \sum_{j=1}^{k-1} g(H_j)$	All the clusters $s_{1:k-1}$.

(22)

A.2. Prior and Likelihood

Remember from Section 4 that, having generated $k-1$ clusters $s_{1:k-1}$, the elements of s_k are generated in a process with latent variables d_k, \mathbf{z}_k and joint distribution

$$p_\theta(\mathbf{s}_k, \mathbf{z}_k, d_k | \mathbf{s}_{1:k-1}, \mathbf{x}) = p_\theta(\mathbf{b}_k | \mathbf{z}_k, \mathbf{x}_k) p_\theta(\mathbf{z}_k | \mathbf{x}_k) p(d_k | \mathbf{s}_{1:k-1}) \quad (23)$$

where

$$p_\theta(\mathbf{b}_k | \mathbf{z}_k, \mathbf{x}_k) = \prod_{i=1}^{m_k} p_{\theta, i}(b_i | \mathbf{z}_k, \mathbf{x}_k). \quad (24)$$

The priors and likelihood are

$$p(d_k | \mathbf{s}_{1:k-1}) = \begin{cases} 1/|I_k| & \text{for } d_k \in I_k, \\ 0 & \text{for } d_k \notin I_k, \end{cases} \quad (25)$$

$$p_\theta(\mathbf{z}_k | \mathbf{x}_k) = \mathcal{N}(\mathbf{z}_k | \mu(\mathbf{x}_k), \sigma(\mathbf{x}_k)) \quad (26)$$

$$p_{\theta, i}(b_i | \mathbf{z}_k, \mathbf{x}_k) = \text{sigmoid}[\rho_i(\mathbf{z}_k, \mathbf{x}_k)] \quad (27)$$

and can be defined in terms of

$$\mu(\mathbf{x}_k) = \mu(D_k, A_k, G_k) \quad (28)$$

$$\sigma(\mathbf{x}_k) = \sigma(D_k, A_k, G_k), \quad (29)$$

$$\rho_i(\mathbf{z}_k, \mathbf{x}_k) = \rho(\mathbf{z}_k, x_{a_i}, D_k, A_k, G_k) \quad i = 1 \dots m_k \quad (30)$$

where μ, σ, ρ are represented with MLPs. Note that in all the cases the functions depend on encodings in (22) that are consistent with the permutation symmetries dictated by the conditioning information.

A.3. ELBO

The ELBO that we want to maximize is given by

$$\mathbb{E}_{p(\mathbf{x}, \mathbf{s}_{1:K})} \log p_\theta(\mathbf{s}_{1:K} | \mathbf{x}) \quad (31)$$

$$= \mathbb{E}_{p(\mathbf{x}, \mathbf{s}_{1:K})} \sum_{k=1}^K \log \left[\sum_{d_k=1}^{N_k} \int d\mathbf{z}_k p_\theta(\mathbf{s}_k, \mathbf{z}_k, d_k | \mathbf{s}_{1:k-1}, \mathbf{x}) \right] \quad (32)$$

$$\geq \mathbb{E}_{p(\mathbf{x}, \mathbf{s}_{1:K})} \sum_{k=1}^K \mathbb{E}_{q_\phi(\mathbf{z}_k, d_k | \mathbf{s}_{1:k}, \mathbf{x})} \log \left[\frac{p_\theta(\mathbf{s}_k, \mathbf{z}_k, d_k | \mathbf{s}_{1:k-1}, \mathbf{x})}{q_\phi(\mathbf{z}_k, d_k | \mathbf{s}_{1:k}, \mathbf{x})} \right] \quad (33)$$

$$= \mathbb{E}_{p(\mathbf{x}, \mathbf{s}_{1:K})} \sum_{k=1}^K \mathbb{E}_{q_\phi(\mathbf{z}_k, d_k | \mathbf{s}_{1:k}, \mathbf{x})} \log \left[\frac{p_\theta(\mathbf{b}_k | \mathbf{z}_k, \mathbf{x}_k) p_\theta(\mathbf{z}_k | \mathbf{x}_k) p(d_k | \mathbf{s}_{1:k-1})}{q_\phi(\mathbf{z}_k | \mathbf{b}_k, d_k, \mathbf{x}_k) q_\phi(d_k | \mathbf{s}_{1:k}, \mathbf{x})} \right] \quad (34)$$

where we introduced the posterior $q_\phi(\mathbf{z}_k, d_k | \mathbf{s}_{1:k}, \mathbf{x}) = q_\phi(\mathbf{z}_k | \mathbf{b}_k, d_k, \mathbf{x}_k) q_\phi(d_k | \mathbf{s}_{1:k}, \mathbf{x})$. For the first factor we assume a form

$$q_\phi(\mathbf{z}_k | \mathbf{b}_k, d_k, \mathbf{x}_k) = \mathcal{N}(\mathbf{z}_k | \mu_q(D_k, A_k^{in}, A_k^{out}, G_k), \sigma_q(D_k, A_k^{in}, A_k^{out}, G_k)) \quad (35)$$

where μ_q, σ_q are MLPs. The most challenging aspect of maximizing the ELBO concerns the factor $q_\phi(d_k | \mathbf{s}_{1:k}, \mathbf{x})$, a multinomial over the N_k components of s_k for which we consider next two different approaches.⁴

A.4. Gumbel-Softmax Relaxation

We start by modeling

$$q_\phi(d_k = s_{k,i} | \mathbf{s}_{1:k}, \mathbf{x}) = \text{Softmax}[\varphi(x_{s_{k,i}}, S_k, A_k^{out}, G_k)] \quad i = 1 \dots N_k \quad (37)$$

Following (Jang et al., 2016; Maddison et al., 2016), we define

$$y_i = \frac{e^{(\varphi_i + g_i)/\tau}}{\sum_{j=1}^{N_k} e^{(\varphi_j + g_j)/\tau}} \quad (38)$$

where τ is a temperature parameter, g_i 's are samples from the Gumbel distribution and

$$\varphi_i = \varphi(x_{s_{k,i}}, S_k, A_k^{out}, G_k). \quad (39)$$

The y_i 's samples are a relaxed version of one-hot samples of d_k from (37) that live in the N_k -simplex. To apply the relaxation of d_k , we just replace $\delta_{s_{k,i}, d_k}$ with y_i in the definitions of D_k and A_k^{in} . Following the recommendation of (Maddison et al., 2016), we express the ELBO in terms of

$$t_i = \log(y) \quad (40)$$

⁴ A third alternative would be to model $q_\phi(d_k | \cdot)$ as (37) and compute the expectation exactly

$$\mathbb{E}_{p(\mathbf{x}, \mathbf{s}_{1:K})} \sum_{k=1}^K \sum_{i=1}^{N_k} q_\phi(d_k = s_{k,i} | \mathbf{s}_{1:k}, \mathbf{x}) \mathbb{E}_{q_\phi(\mathbf{z}_k | \mathbf{b}_k, d_k, \mathbf{x}_k)} \log \left[\frac{p_\theta(\mathbf{b}_k | \mathbf{z}_k, \mathbf{x}_k) p_\theta(\mathbf{z}_k | \mathbf{x}_k) p(d_k | \mathbf{s}_{1:k-1})}{q_\phi(\mathbf{z}_k | \mathbf{b}_k, d_k, \mathbf{x}_k) q_\phi(d_k | \mathbf{s}_{1:k}, \mathbf{x})} \right] \quad (36)$$

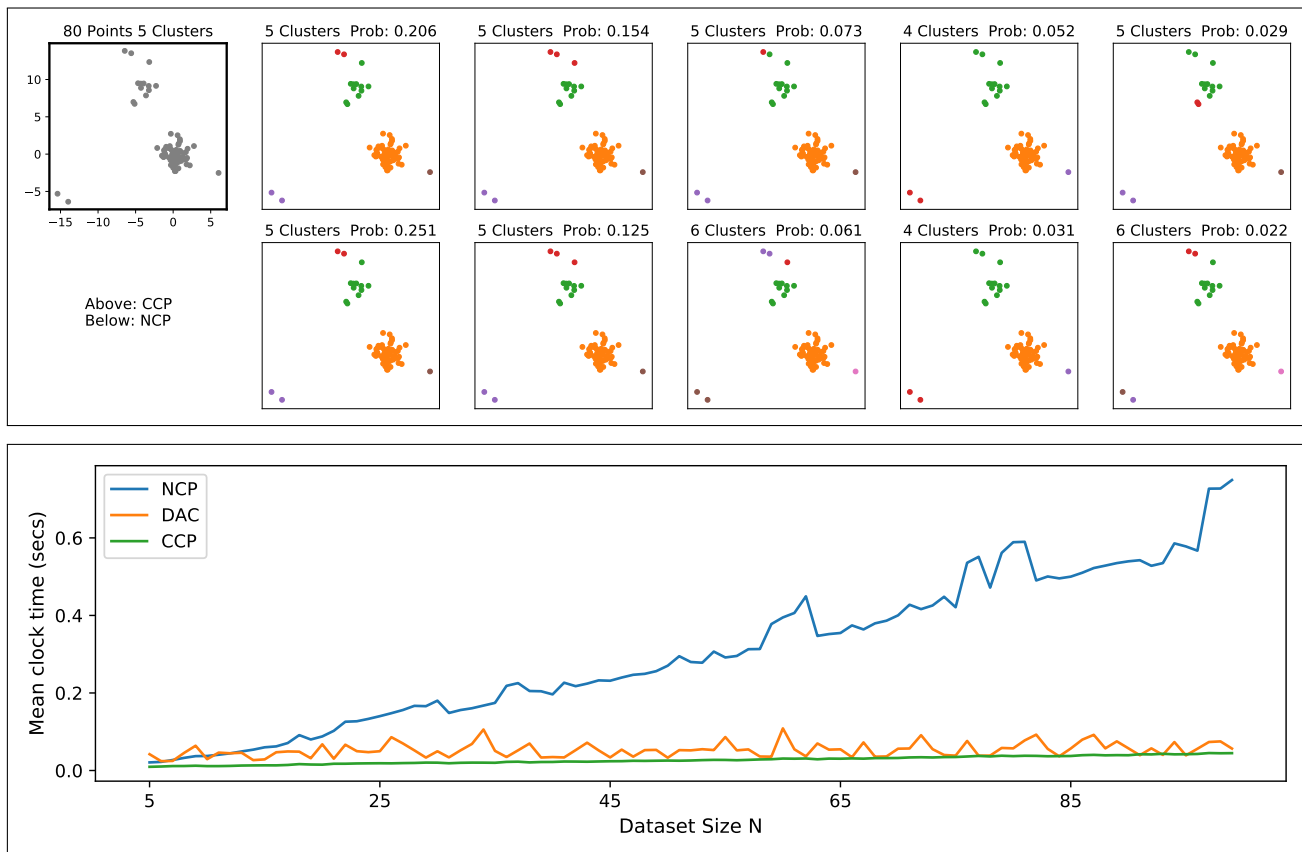


Figure S1. **Comparing Samples and Times.** Above: Samples from NCP and CCP on the same data set. Both models were trained using the generative model for mixtures of 2D Gaussians from Section 5. Note that the higher probability clusters agree in their labels and approximately in the assigned probabilities. Below: Clock time as a function of the dataset size for NCP, CCP and DAC (Lee et al., 2019),⁶ all trained and tested with the same 2D Gaussian model as above. Each point in the curve is the average over 25 datasets. For NCP and CCP we sampled 200 full posterior samples, while DAC gives a single deterministic output.

Calling $\kappa_{g,\tau}(t)$ their probability density (see (Maddison et al., 2016) for the explicit form), the relaxed ELBO becomes

$$\mathbb{E}_{p(\mathbf{x}, \mathbf{s}_{1:K})} \sum_{k=1}^K \mathbb{E}_{q_\phi(\mathbf{z}_k, \mathbf{y} | \mathbf{s}_{1:k}, \mathbf{x})} \log \left[\frac{\prod_{i=1}^{N_k} [p_{\theta,i}(b_i = 1 | \mathbf{z}_k, \mathbf{y})]^{1-y_i} \prod_{i=1, b_i=0}^{m_k} p_{\theta,i}(b_i = 0 | \mathbf{z}_k, \mathbf{y}) p_\theta(\mathbf{z}_k | \mathbf{y})}{q_\phi(\mathbf{z}_k | \mathbf{y}) \kappa_{g,\tau}(t(\mathbf{y}))} \right] + \text{const.}$$

In this relaxed version the reparametrization trick can be used in the usual way to compute derivatives of q_ϕ .

A.5. Uniform Discrete Posterior

A simpler approach to model $q_\phi(d_k | \mathbf{s}_{1:k}, \mathbf{x})$ is by approximating it as uniform, given by

$$q(d_k | \mathbf{s}_{1:k}) = \begin{cases} 1/N_k & \text{for } d_k \in \mathbf{s}_k, \\ 0 & \text{for } d_k \notin \mathbf{s}_k. \end{cases} \quad (41)$$

This approximation is very good in cases of well separated clusters. Since $q(d_k | \mathbf{s}_{1:k})$ has no parameters now, this avoids the problem of backpropagation through discrete variables. In the examples we considered, this simpler approach yielded better results, as measured, e.g., by a better agreement in Geweke’s test (see Figure 5). So this was the approach we adopted in the results we present in this work.

⁶We used the DAC code available at <https://github.com/ICLR2020anonymous/dac>.

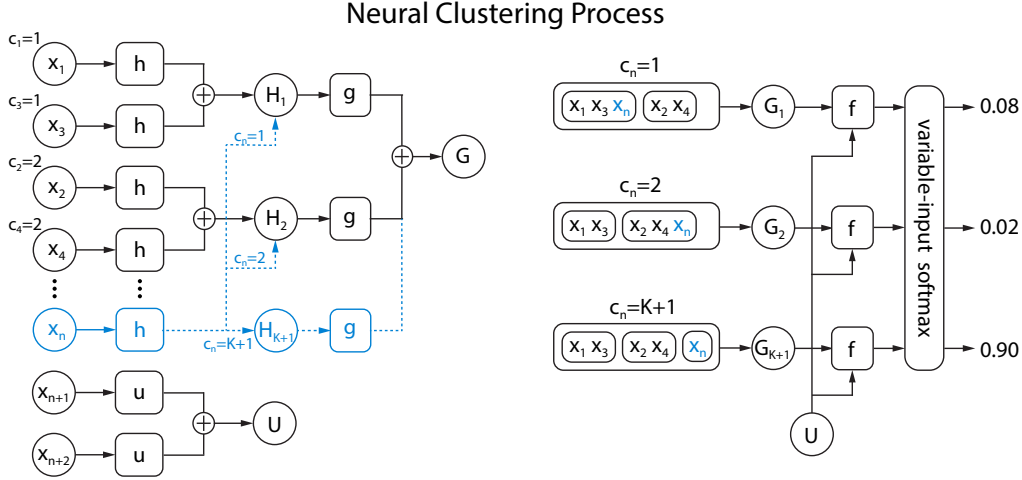


Figure S2. **Architecture of the Neural Clustering Process.** The full model is composed by the deep networks h, g, u, f . *Left:* After assigning the cluster labels $c_{1:n-1}$, each possible discrete value k for c_n gives a different symmetry-invariant encoding of $x_{1:n}$ into the vector G_k , using the functions h and g . The remaining, yet-unassigned points $x_{n+1:N}$ are encoded by u and summed into the vector U . *Right:* Each pair G_k, U is mapped by f into a real number (logit), which in turn is mapped into the multinomial distribution $q_\theta(c_n | c_{1:n-1}, \mathbf{x})$ via a variable-input softmax.

B. Neural Clustering Process for Exponential Families

The details of the NCP architecture are fully explained in Section 3, and Figure S2 shows the architecture diagrammatically.

In the section we consider the spacial case of exponential family likelihoods, given by

$$p(x|\mu) = e^{\mu \cdot t(x) - \psi(\mu)} m(x) \quad (42)$$

$$= e^{\lambda \cdot h(x)} m(x) \quad (43)$$

where $t(x)$ is a vector of sufficient statistics, and we defined

$$h(x) = (1, t(x)) \quad (44)$$

$$\lambda = (-\psi(\mu), \mu) \quad (45)$$

Let us denote by K and $K' \geq K$ the total number of distinct values in $c_{1:n}$ and $c_{1:N}$, respectively. Consider the joint distribution

$$p(c_{1:N}, \mathbf{x}, \mu) = p(c_{1:N}) p(\mu) \prod_{k=1}^{K'} e^{\lambda_k \cdot \sum_{i:c_i=k} h(x_i)} \prod_{i=1}^N m(x_i) \quad (46)$$

from which we obtain the marginal distributions

$$p(c_{1:n}, \mathbf{x}) = \sum_{c_{n+1} \dots c_N} p(c_{1:N}, \mathbf{x}) \quad (47)$$

$$= \sum_{c_{n+1} \dots c_N} \int d\mu p(c_{1:N}) p(\mu) \prod_{k=1}^{K'} e^{\lambda_k \cdot (H_k + \sum_{i>n:c_i=k} h(x_i))} \prod_{i=1}^N m(x_i) \quad (48)$$

$$= F(H_1, \dots, H_K, h(x_{n+1}), \dots, h(x_N)) \prod_{i=1}^N m(x_i) \quad (49)$$

where we defined

$$H_k = \sum_{i \leq n, c_i=k} h(x_i) \quad k = 1 \dots K \quad (50)$$

and $H_k = 0$ for $k > K$.

Note now that if $p(c_{1:N})$ is constant, all the dependence of F on $c_{1:n}, x_{1:n}$ is encoded in the H_k 's, and F is symmetric under separate permutations of the H_k 's and the $h(x_i)$'s for $i > n$. Based on these symmetries we can approximate F as

$$F \simeq e^{f(G,U)} \quad (51)$$

modulo adding to f any function symmetric on all x_i 's, where

$$G = \sum_{k=1}^K g(H_k) \quad (52)$$

$$U = \sum_{i=n+1}^N u(x_i) \quad (53)$$

In the conditional probability we are interested in,

$$p(c_n | c_{1:n-1}, \mathbf{x}) = \frac{p(c_{1:n}, \mathbf{x})}{\sum_{c_n} p(c_{1:n}, \mathbf{x})}, \quad (54)$$

the product of the $m(x_i)$'s in (49) cancels. Similarly, adding to f a function symmetric on all x_i 's leaves invariant our proposed approximation

$$q_\theta(c_n = k | c_{1:n-1}, \mathbf{x}) = \frac{e^{f(G_k, U)}}{\sum_{k'=1}^{K+1} e^{f(G_{k'}, U)}} \quad k = 1 \dots K + 1. \quad (55)$$

C. Monitoring global permutation invariance

As mentioned in Section 7, we must verify the symmetry of the posterior likelihood under global permutations of all the data points. We show such a check in Figure S3.

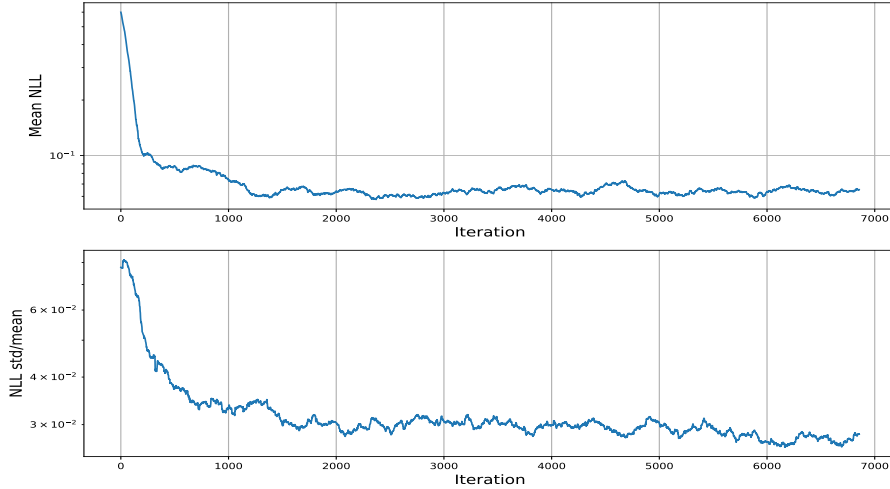


Figure S3. **Global permutation invariance.** Training curves for the NCP model of 2D Gaussians in Section 2. Each minibatch was evaluated for 8 random permutations of the order of the points in the dataset. *Above:* Mean of the NLL over the permutations. *Below:* NLL standard deviation/NLL mean. Note that the ratio is of order 10^{-2} .

D. Details of spike sorting using NCP

Data preprocessing. Training and test data come from the retinal recordings in (Chichilnisky & Kalmar, 2002) using a 512-channel 2D hexagonal MEA with 20 kHz sampling rate. After spike detection (Lee et al., 2017), each multi-channel spike waveform was assigned to the channel where the waveform has the maximum peak-to-peak (PTP) amplitude (i.e. the center channel, ch0). This partitioned the recording data by channel such that each center-channel-based partition only contains multi-channel spike waveforms centered at that channel. Each spike waveform is represented as a 7×32 array containing the 32 time steps surrounding the peak from the center channel and the same time window from the 6 immediate neighbor channels (Figure 6). These 7×32 arrays are the spikes on which clustering was performed.

Neural architecture for NCP spike sorting. The overall architecture is the same as the one described in Section 3 and Figure S2. To extract useful features from the spatial-temporal patterns of spike waveforms, we use a 1D ConvNet as the h and u encoder functions. The convolution is applied along the time axis, with each electrode channel treated as a feature dimension. The ConvNet uses a ResNet architecture (He et al., 2016) with 4 residual blocks, each having 32, 64, 128, 256 feature maps (kernel size = 3, stride = [1, 2, 2, 2]). The last block is followed by an averaged pooling layer and a final linear layer. The outputs of the ResNet encoder are the h_i and u_i vectors of NCP, i.e. $h_i = \text{ResNetEncoder}(x_i)$. We used $d_h = d_u = 256$. The other two functions, g and f , are identical to those in the 2D Gaussian example.

Training NCP using synthetic data. To train NCP for spike clustering, we created synthetic labeled training data using a MFM generative model (Miller & Harrison, 2018) of noisy spike waveforms that mimic the distribution of real spikes:

$$N \sim \text{Uniform}[N_{min}, N_{max}] \quad (56) \quad c_1 \dots c_N \sim \text{Cat}(\pi_1, \dots, \pi_K) \quad (59)$$

$$K \sim 1 + \text{Poisson}(\lambda) \quad (57) \quad \mu_k \sim p(\mu) \quad k = 1 \dots K \quad (60)$$

$$\pi_1 \dots \pi_K \sim \text{Dirichlet}(\alpha_1, \dots, \alpha_K) \quad (58) \quad x_i \sim p(x_i | \mu_{c_i}, \Sigma_s \otimes \Sigma_t) \quad i = 1 \dots N \quad (61)$$

Here, N is the number of spikes between [200, 500]. The number of clusters K is sampled from a shifted Poisson distribution with $\lambda = 2$ so that each channel has on average 3 clusters. $\pi_{1:K}$ represents the proportion of each cluster and is sampled from a Dirichlet distribution with $\alpha_{1:K} = 1$. The training spike templates $\mu_k \in \mathbb{R}^{7 \times 32}$ are sampled from a reservoir of 957 ground-truth templates not present in any test data, with the temporal axis slightly jittered by random resampling. Finally, each waveform x_i is obtained by adding to μ_{c_i} Gaussian noise with covariance given by the Kronecker product of spatial and temporal correlation matrices estimated from the training data. This method creates spatially and temporally correlated noise patterns similar to real data (Figure S4). We trained NCP for 20000 iterations on a GPU with a batch size of 32 to optimize the NLL loss by the Adam optimizer (Kingma & Ba, 2015). A learning rate of 0.0001 was used (reduced by half at 10k and 17k iterations).

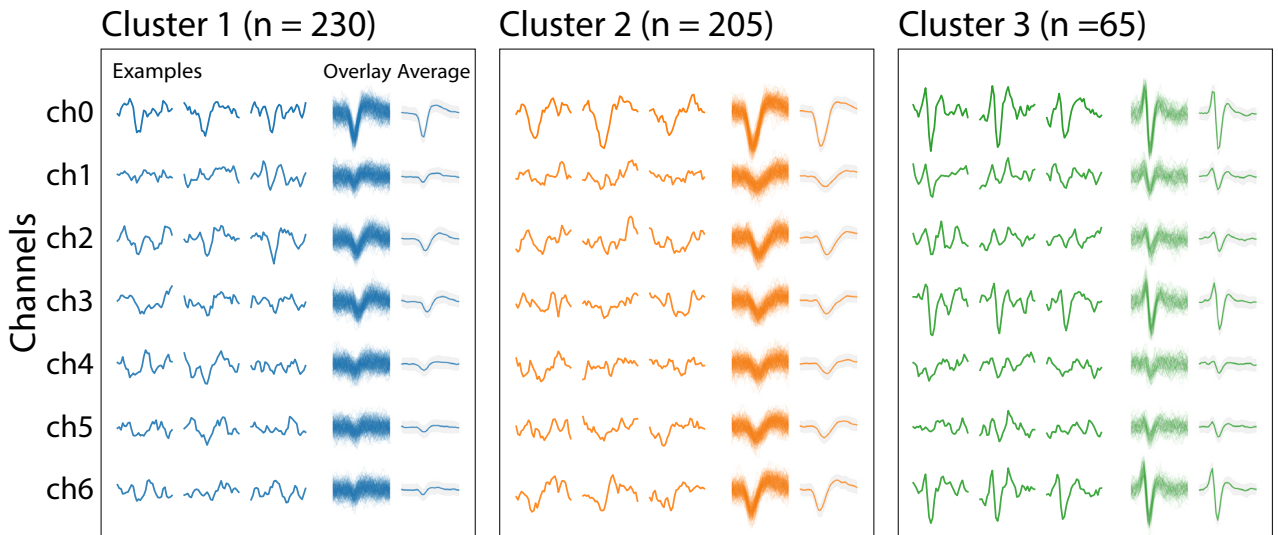


Figure S4. **Synthetic data examples.** Example of 500 synthetic spikes from 3 clusters.

Probabilistic spike clustering using NCP. At inference time, we fed the 7 x 32 arrays of spike waveforms to NCP, and performed GPU-parallelized posterior sampling of cluster labels (Figure S2 and Figure 6). Using beam search (Graves, 2012; Sutskever et al., 2014) with a beam size of 150, we were able to efficiently sample 150 high-likelihood clustering configurations for 2000 spikes in less than 10 seconds on a single GPU. After clustering, we obtained a spike template for each cluster as the average shape of the spike waveforms. The clustering configuration with the highest probability was used for most experiments.

The spike sorting pipelines for real and hybrid data. The real data is a 49-channel, 20-minute retina recording with white noise stimulus. To create the hybrid test data, 20 ground-truth spike templates were manually selected from a 49-channel test recording and inserted into another test dataset according to the original spike times.

For NCP and vGMFM, we performed clustering on 2000 randomly sampled spikes from each channel (clusters containing less than 20 spikes were discarded), and assigned all remaining spikes to a cluster based on the L2 distance to the cluster centers. Then, a final set of unique spike templates were computed, and each detected spike was assigned to one of the templates. The clustering step of vGMFM uses the first 5 PCA components of the spike waveforms as input features. For Kilosort, we run the entire pipeline using the Kilosort2 package (Pachitariu, 2019). After extracting spike templates and RFs from each pipeline, we matched pairs of templates from different methods by L-infinity distance and pairs of RFs by cosine distance.

Electrode drift in real MEA data. The NCP spike sorting pipeline described above does not take into consideration electrode drift over time, which is present in some real recording data. As a step towards addressing the problem of spike sorting in the presence of electrode drift (Calabrese & Paninski, 2011; Shan et al., 2017), we describe in Sup. Material F a generalization of NCP to handle data in which the per-cluster parameters (e.g. the cluster means) are nonstationary in time.

E. Experimental results for NCP spike sorting

Synthetic Data. We run NCP and vGMFM on 20 sets of synthetic test data each with 500, 1000, and 2000 spikes. As the ground-truth cluster labels are known, we compared the clustering quality using Adjusted Mutual Information (AMI) (Vinh et al., 2010). The AMI of NCP is on average 11% higher than vGMFM (SM Figure S5), showing better performance of NCP on synthetic data.

Real Data. We run NCP, vGMFM and Kilosort on a retina recording with white noise stimulus as described in SM Section D, and extracted the averaged spike template of each cluster (i.e. putative neuron). Example clustering results in SM Figure S6 (top) show that NCP produces clean clusters with visually more distinct spike waveforms compared to vGMFM. As real data do not come with ground-truth cluster labels, we compared the spike templates extracted from NCP and Kilosort using retinal receptive field (RF), which is computed for each cluster as the mean of the stimulus present at each spike. A clearly demarcated RF provides encouraging evidence that the spike template corresponds to a real neuron. Side-by-side comparisons of matched RF pairs are shown in SM Figure S6 (bottom-left) and SM Figure S8. Overall, NCP found 103 templates with clear RFs, among which 48 were not found by Kilosort, while Kilosort found 72 and 17 of them were not found by NCP (SM Figure S6 bottom-right). Thus NCP performs at least as well as Kilosort, and finds many additional templates with clear RFs.

Hybrid Data. We compared NCP against vGMFM and Kilosort on a hybrid recording with partial ground truth as in (Pachitariu et al., 2016). Spikes from 20 ground-truth templates were inserted into a real recording to test the spike sorting performance on realistic recordings with complex background noise and colliding spikes. As shown in SM Figure S7, NCP recovered 13 of the 20 injected ground-truth templates, outperforming both Kilosort and vGMFM, which recovered 8 and 6, respectively.

Neural Clustering Processes

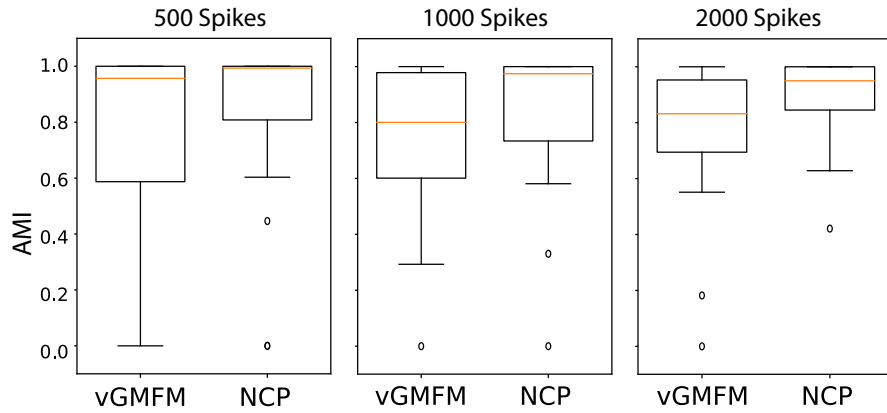


Figure S5. **Clustering synthetic data.** The AMI scores for clustering 20 sets of 500, 1000, and 2000 unseen synthetic spikes.

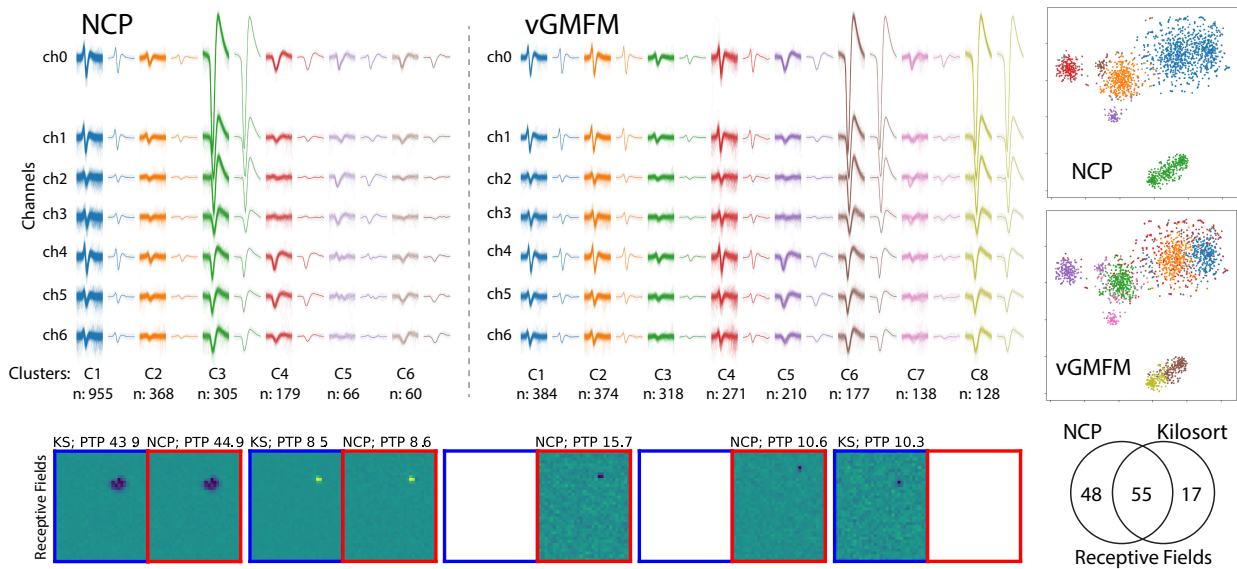


Figure S6. **Spike sorting on real data.** 2000 spikes from real data were clustered by NCP (*top-left*) and vGMFM (*top-mid*). Each column shows the spikes assigned to one cluster (overlying traces and their average). Each row is one electrode channel. *Top-right*: t-SNE visualization of the spike clusters. *Bottom-left*: Example pairs of matched RFs recovered by NCP (red boxes) and Kilosort (blue boxes). Blank indicates no matched counterpart. *Bottom-right*: Venn diagram of recovered RFs.

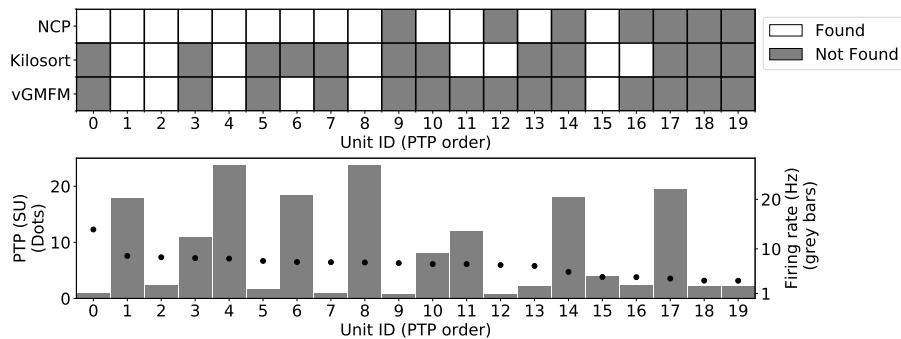


Figure S7. **Spike sorting on hybrid data.** *Top*: NCP, Kilosort, vGMFM recovered 13, 8, and 6 of the 20 injected ground-truth templates. *Bottom*: Peak-to-peak (PTP) size and firing rate of each injected template. (Smaller templates with lower firing rates are more challenging.)

Neural Clustering Processes

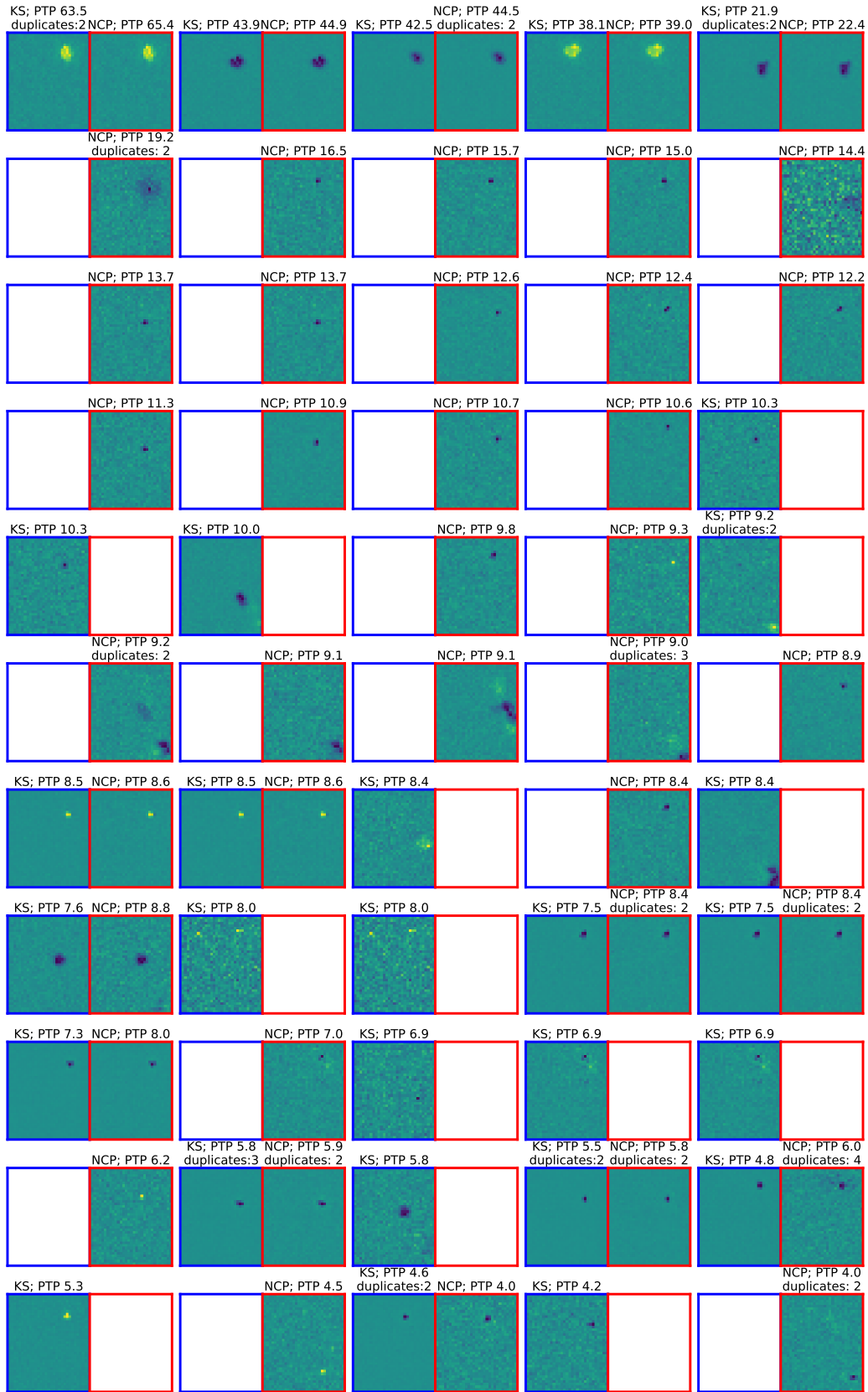


Figure S8. **Spike sorting on real data.** Receptive fields of 55 randomly selected pairs of units recovered from Kilosort and NCP spike sorting. (Red boxes indicate units found by NCP; blue boxes by Kilosort.) Both approaches find the spikes with the biggest peak-to-peak (PTP) size. For smaller-PTP units often one sorting method finds a cell that the other sorter misses. NCP and KS find a comparable number of units with receptive fields here, with NCP finding a few more than KS; see text for details.

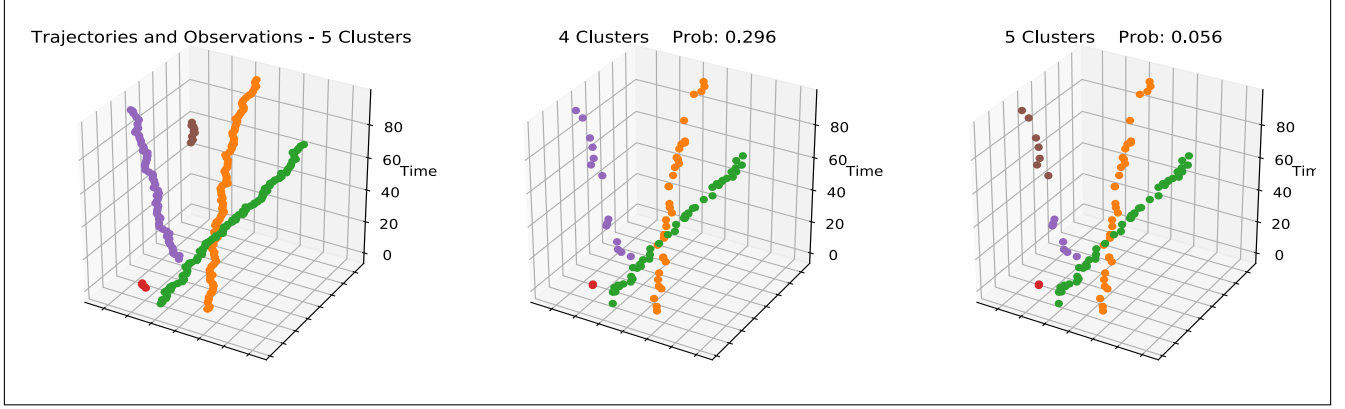


Figure S9. **Neural Particle Tracking.** *Left:* Time trajectories of 5 2D particles. Note that particles can appear or disappear at arbitrary times. *Middle and right:* Two posterior samples. Note that since only one particle is observed at each time, a particle not observed for some time leads to a possible ambiguity on the number of particles. (Best seen in color.)

F. Particle tracking

Inspired by the problem of electrode drift (Calabrese & Paninski, 2011; Pachitariu, 2019; Shan et al., 2017), let us consider now a generative model given by

$$c_t \sim p(c_t | c_1, \dots, c_{t-1}) \quad t = 1, \dots, T \quad (62)$$

$$\mu_{k,t} \sim p(\mu_{k,t} | \mu_{k,t-1}) \quad k = 1 \dots K \quad t = 1, \dots, T \quad (63)$$

$$x_t \sim p(x_t | \mu_{c_t,t}) \quad t = 1, \dots, T \quad (64)$$

In this model, a cluster corresponds to the points along the time trajectory of a particle, and (63) represents the time evolution of the cluster parameters. The cluster labels c_t indicate which particle is observed at time t , and note that particles can in principle appear or disappear at any time.

To take the time evolution into account, we let particles influence one another with a weight that depends on their time distance. For this, let us introduce a time-decay constant $b > 0$, and generalize the NCP equations to

$$H_{k,t} = \sum_{t'=1:c_{t'}=k}^t e^{-b|t-t'|} h(x_{t'}) \quad k = 1 \dots K, \quad (65)$$

$$G_t = \sum_{k=1}^K g(H_{k,t}), \quad (66)$$

$$U_t = \sum_{t'=t+1}^T e^{-b|t-t'|} u(x_{t'}). \quad (67)$$

The conditional assignment probability for c_t is now

$$q_\theta(c_t = k | c_{1:t-1}, \mathbf{x}) = \frac{e^{f(G_{k,t}, U_t)}}{\sum_{k'=1}^{K+1} e^{f(G_{k',t}, U_t)}} \quad (68)$$

for $k = 1 \dots K + 1$. The time-decay constant b is learnt along with all the other parameters. We can also consider replacing $e^{-b|t-t'|}$ with a general distance function $e^{-d(|t-t'|)}$. Figure S9 illustrates this model in a simple 2D example. We call this approach Neural Particle Tracking.

G. Neural architectures in the examples

To train the networks in the examples, we used stochastic gradient descent with Adam (Kingma & Ba, 2015), with learning rate 10^{-4} . The number of samples in each mini-batch were: 1 for $p(N)$, 1 for $p(c_{1:N})$, 64 for $p(\mathbf{x} | c_{1:N})$. The architecture

of the functions in each case were:

NCP: 2D Gaussians

- h : MLP [2-256-256-256-128] with ReLUs
- u : MLP [2-256-256-256-128] with ReLUs
- g : MLP [128-256-256-256-256] with ReLUs
- f : MLP [384-256-256-256-1] with ReLUs

NCP: MNIST

- h : 2 layers of [convolutional + maxpool + ReLU] + MLP [320-256-128] with ReLUs
- u : same as h
- g : MLP [256-128-128-128-128-256] with ReLUs
- f : MLP [384-256-256-256-1] with ReLUs